Energy Reports 14 (2025) 2670–2685

Contents lists available at ScienceDirect

Energy Reports

journal homepage: www.elsevier.com/locate/egyr

Research paper

Optimization of control-oriented AI models for real-time platform pitch prediction in hybrid wind-wave offshore systems

Irfan Ahmad [a,*], Mehdi Neshat [b], Aitor Garrido [a], Izaskun Garrido [a]

[a] Automatic Control Group - ACG, Inst. of Research and Development of Processes - IIDP, Department of Automatic Control and Systems, Engineering School of Bilbao – EIB/BIE, University of the Basque Country, UPV/EHU, Rafael Moreno 3, 48013, Bilbao, Spain

[b] Faculty of Engineering and Information Technology, University of Technology Sydney, Ultimo, Sydney, 2007, NSW, Australia

ARTICLE INFO

Keywords:
Offshore wind
Wave energy
Hybrid systems
Deep learning
Predictive modeling
Platform pitch
Real-time control
CNN
LSTM
FSST

ABSTRACT

This study presents a control-oriented deep learning framework for real-time prediction of platform pitch motion in hybrid offshore wind-wave systems. The core contribution lies in a hybrid CNN-LSTM architecture augmented with time–frequency features derived from the fourier synchrosqueezed transform (FSST). This integrated design enables simultaneous spatial pattern recognition, temporal sequence modeling, and spectral enrichment, capturing complex nonlinear dynamics inherent to multivariate time series data. Trained on high-fidelity OpenFAST simulation data, the proposed model achieves a root mean square error (RMSE) of 0.26 degrees with an inference latency of 15 ms, outperforming conventional physics-based and standalone neural models by a factor of 6.4.

Robustness is demonstrated across diverse operating conditions, with sensitivity analyses confirming stable predictive performance under varying wave heights, wind speeds, and control inputs. In addition to accuracy, the study addresses deployment feasibility on embedded hardware, model interpretability, and readiness for integration with model predictive control (MPC) architectures. Key limitations, such as generalizability to extreme conditions and explainability, are critically examined, offering a roadmap for future enhancements.

By bridging simulation-based learning with real-time control demands, this work advances the applicability of deep learning in offshore renewable energy platforms. It provides a scalable, low-latency, and accurate solution for intelligent vibration mitigation and next-generation control of floating hybrid systems.

1. Introduction

The transition to renewable energy sources is essential for mitigating climate change, reducing greenhouse gas emissions, and ensuring long-term energy security. Offshore wind energy has emerged as a critical component in this transformation, offering higher and more stable wind speeds than land-based alternatives. In regions like Europe, sustained policy support and continuous technological advancements have enabled the rapid deployment of large-scale offshore wind farms (Li et al., 2023). Innovations in floating support structures and marine energy conversion technologies further reinforce offshore wind's central role in the global clean energy landscape (Al-Ismail et al., 2023).

FOWTs extend offshore wind exploitation to deep-sea regions previously inaccessible to fixed-bottom turbines. These systems capitalize on stronger and more consistent wind profiles, thereby improving energy yield and integration into the power grid. However, the inherent buoyancy of floating platforms makes them susceptible to six degrees-of-freedom (6-DOF) motion, particularly pitch, roll, and heave. These oscillatory dynamics compromise power quality, increase fatigue loading, and complicate control system design. Addressing these motion-induced instabilities demands advanced control strategies capable of operating under nonlinear and time-varying environmental conditions. The offshore wind industry is projected to experience significant growth in the coming years. As depicted in Fig. 1, the market size is expected to grow rapidly, reaching $104.95B by 2029 with a CAGR of 15.90%.

Wave energy offers a complementary renewable resource that can balance the intermittency of wind energy. Among various wave energy converter (WEC) designs, OWC stands out due to its structural simplicity, effective pneumatic energy conversion, and potential synergy with floating platforms. When integrated with FOWTs, OWCs not only contribute to hybrid energy generation but also help attenuate platform motion by dissipating wave energy through air chamber dynamics (Aboutalebi et al., 2021). Such hybrid systems can thus enhance

* Corresponding author.
E-mail addresses: irfan.ahmad@ehu.eus (I. Ahmad), mehdi.neshat@uts.edu.au (M. Neshat), aitor.garrido@ehu.eus (A. Garrido), izaskun.garrido@ehu.eus (I. Garrido).

https://doi.org/10.1016/j.egyr.2025.09.006
Received 6 May 2025; Received in revised form 27 August 2025; Accepted 17 September 2025
Available online 26 September 2025

Nomenclature

Acronyms		Symbols	
ANN	Artificial Neural Network	$\theta(t)$	Platform pitch angle [deg]
CNN	Convolutional Neural Network	ω	Angular frequency [rad/s]
DANN	Deep Artificial Neural Network	$H_s(t)$	Significant wave height [m]
EMD	Empirical Mode Decomposition	T_p	Peak wave period [s]
FFT	Fast Fourier Transform	U	Wind speed [m/s]
FOWT	Floating Offshore Wind Turbine	TI	Turbulence intensity [%]
FSST	Fourier Synchrosqueezed Transform	β_p	Blade pitch angle [deg]
LSTM	Long Short-Term Memory	f_c	Filter cutoff frequency [Hz]
MAE	Mean Absolute Error	η	Learning rate
MPC	Model Predictive Control	B	Batch size
OWC	Oscillating Water Column	E	Number of epochs
RMSE	Root Mean Square Error	$V_w(t)$	Wind speed [m/s]
RNN	Recurrent Neural Network	$V_{\text{ctrl}}(t)$	Control voltage signal [V]
STFT	Short-Time Fourier Transform		
WEC	Wave Energy Converter		
WT	Wavelet Transform		

energy capture, improve operational stability, and optimize overall platform performance.

The integration of Oscillating Water Columns with Floating Offshore Wind Turbines introduces complex, coupled dynamics that span aerodynamic forces, hydrodynamic loading, structural behavior, and control system interactions. Conventional modeling techniques—such as linearized potential flow theory and simplified coupled simulation frameworks are often inadequate in capturing the full range of nonlinear phenomena associated with wind and wave interactions, including viscous damping, resonance effects, and stochastic environmental excitations (Neshat et al., 2024a). Recent studies have employed artificial intelligence-based approaches for nonlinear system identification and performance modeling [Madiastuty et al., 2023; Ahmad et al., 2024], while others have proposed control optimization frameworks and coupled dynamic simulations for floating hybrid platforms [Xue et al., 2025; Liu et al., 2024b; Han et al., 2024; Ahmad et al., 2025]. Additional contributions have focused on experimental validation and the dynamic behavior of various configurations under operational and extreme marine conditions [Ding et al., 2024; Hua et al., 2025; Wei et al., 2025]. Despite these advancements, there remains a critical research gap: the lack of real-time, control-oriented predictive models that can accurately estimate the platform's pitch motion in offshore environments while maintaining low computational demands. The present study addresses this challenge by introducing a deep learning-based surrogate model that integrates convolutional neural networks for spatial pattern recognition with long short-term memory networks for temporal sequence prediction, trained using high-fidelity simulation data from open-source offshore simulation tools.

1.1. Literature review and research gaps

Recent research has increasingly focused on data-driven methods, particularly deep learning, for modeling complex dynamic behaviors of offshore structures. Notable studies have applied Artificial Neural Networks, recurrent neural networks (RNNs), and LSTM networks to predict floating platform motions with enhanced accuracy (Shi et al., 2023; Liu et al., 2024a; Chen et al., 2022). For example, Shi et al. (2023) developed a Multi-Input LSTM model that integrates multiple environmental variables, achieving substantial improvements in motion prediction. Similarly, Liu et al. (2024a) combined empirical mode decomposition (EMD) with neural networks, reporting coefficient of determination (R^2) values consistently above 0.5 across diverse maritime conditions. Wei et al. (2013) demonstrated that hybrid wavelet-neural network models outperform traditional ANN models in capturing complex offshore time-series data, laying the groundwork for advanced response forecasting.

Hybrid approaches that fuse physics-informed principles with data-driven techniques have also gained attention. Wang et al. (2023) introduced physics-informed neural networks (PINNs) incorporating simplified hydrodynamic constraints, resulting in root mean square errors approximately 15% lower than conventional data-driven counterparts. Chen et al. (2022) proposed deep neural operators capable of real-time response prediction for floating offshore structures, offering accuracy comparable to physics-based methods but with significantly reduced computational cost. Despite these advancements, challenges remain in achieving a balance between accuracy, computational efficiency, and robustness across varied operational conditions. Recent advancements in data-driven forecasting and hybrid optimization have significantly enhanced the modeling of wave and hybrid energy systems, including meta-learner-based wave power prediction using deep gradient boosting (Neshat et al., 2024b), adaptive bi-level whale optimization for maximizing hybrid wind-wave output (Neshat et al., 2024c), and decomposition-based convolutional bidirectional frameworks for wave energy forecasting (Neshat et al., 2022).

Previous research on hybrid offshore platforms has largely focused on structural optimization (Liu et al., 2022) and basic control methods (Han et al., 2023), often relying on simplified hydrodynamic models that fall short in capturing the nonlinear wave-structure interactions crucial for accurate motion prediction. While Liu et al. (2022) and Han et al. (2023) improved power capture through control optimization, their approaches depend on computationally expensive simulations—taking over 30 min for a 10 min window. Similarly, dynamic models by Zhang et al. (2022) and Karimi et al. (2024) offer detailed behavior insights but lack predictive control features. Table 1 summarizes recent progress in modeling, control, and optimization of hybrid wind-wave platforms, covering both physics-based and data-driven approaches.

Prior investigations into hybrid offshore platforms predominantly address structural design optimization (Liu et al., 2022) and fundamental control strategies (Han et al., 2023). However, many rely on simplified hydrodynamic models that inadequately capture nonlinear wave-structure interactions essential for precise motion prediction. Control optimization frameworks by Liu et al. (2022) and Han et al. (2023) demonstrate improved power capture but depend on computationally intensive physics-based simulations, with reported runtimes exceeding 30 min for a 10 min simulation window. Coupled dynamic simulations by Zhang et al. (2022) and Karimi et al. (2024) provide detailed platform behavior insights but lack predictive control capabilities necessary for advanced stabilization. Table 1 provides a comprehensive summary of recent advancements in control, modeling, and optimization strategies for hybrid floating wind-wave systems, highlighting both data-driven and simulation-based approaches.

Existing studies in FOWT-OWC stabilization largely rely on simplified linearized models or computationally intensive numerical simulations that, while insightful, lack comprehensive control-oriented frameworks (M'zoughi et al., 2024, 2022). Many works focus on either

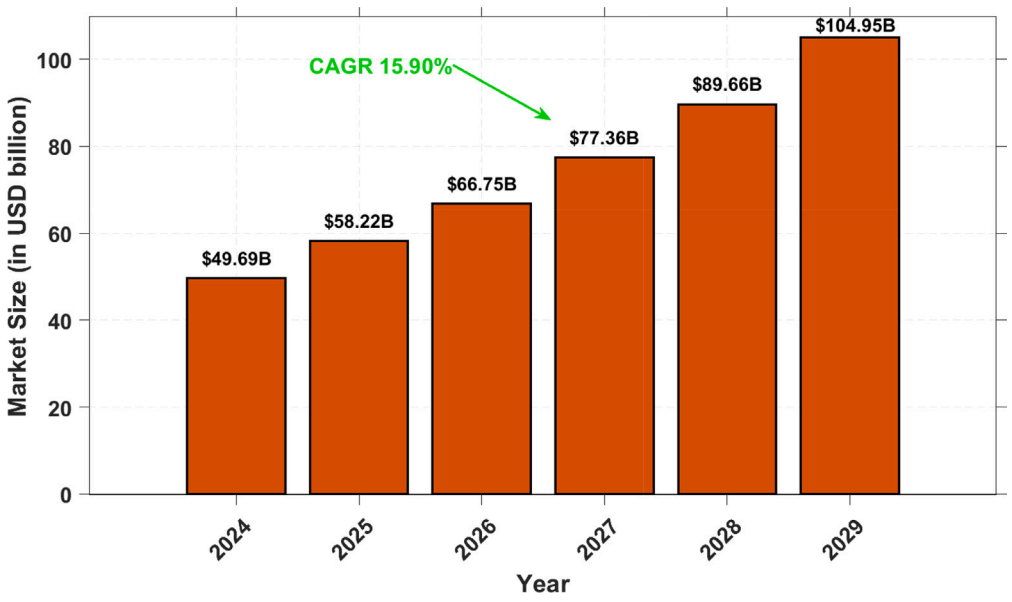

Fig. 1. Offshore wind global market report 2025. The market size is expected to reach $104.95B by 2029 with a CAGR of 15.90%.

basic control strategies or empirical validations without integrating advanced data-driven methods tailored for real-time prediction and control (Ahmad et al., 2024a; M'zoughi et al., 2021). Our study fills this critical gap by presenting a hybrid CNN-LSTM model enriched with spectral feature extraction, achieving over 80% reduction in RMSE with computational efficiency compatible with real-time control. The research addresses critical gaps in computational efficiency and prediction fidelity, offering a viable pathway for enhancing the control and operational efficiency of complex offshore energy systems.

These limitations reveal several critical research gaps:

1. **Control-Oriented Modeling Deficiency**: There is a pressing need for simplified, computationally efficient control-oriented models that facilitate the implementation of advanced control schemes without sacrificing essential nonlinear dynamics.
2. **Computational Efficiency Gap**: High-fidelity physics-based models entail excessive computational cost (minutes to hours), hindering their feasibility for real-time control applications.
3. **Fidelity-Speed Trade-off**: Existing models tend to compromise between accuracy and real-time applicability, often favoring one at the expense of the other.
4. **Adaptability Limitations**: Many models are optimized for narrow operational conditions and lack robustness over the broad range of offshore environmental variability.
5. **Feature Engineering Limitations**: Traditional time-domain features inadequately capture the frequency-dependent complexities of wave-structure interactions, restricting model generalizability.

1.2. Research hypothesis and contributions

Building upon the identified research gaps, we hypothesize that a hybrid deep learning architecture – combining Convolutional Neural Networks for effective spatial feature extraction and LSTM networks for modeling temporal dependencies – augmented with advanced spectral features derived from the FSST, can effectively bridge the current limitations. This integrated approach aims to deliver real-time, high-fidelity platform pitch predictions while preserving physical interpretability and ensuring operational robustness across diverse offshore conditions.

Specifically, the study posits that such a CNN-LSTM-FSST hybrid model will achieve a minimum fivefold improvement in prediction accuracy over conventional physics-based and purely data-driven methods, concurrently maintaining inference times below 20 ms, thereby meeting the stringent requirements of real-time model predictive control (MPC) implementations.

The principal contributions of this work are as follows:

1. The development of a novel hybrid CNN-LSTM architecture customized for offshore platform pitch prediction, effectively integrating spatial and temporal learning capabilities.
2. The introduction of FSST-based spectral feature engineering to enhance the model's performance by providing superior time–frequency resolution of input signals.
3. Comprehensive optimization and validation of the proposed control-oriented model using high-fidelity simulation data generated by OpenFAST.
4. Demonstration of real-time prediction capabilities with inference times below 15 ms, alongside significantly improved accuracy relative to benchmark models.
5. In-depth analysis of the model's robustness, generalizability, computational efficiency, and practical integration challenges pertinent to offshore deployment.

This study therefore, presents a technically rigorous, robust, and control-oriented predictive modeling framework that leverages deep learning to estimate platform pitch motion within hybrid floating offshore wind systems integrated with oscillating water columns. Distinct from traditional physics-based formulations, the proposed data-driven methodology offers real-time inference with minimal parameterization, rendering it highly suitable for dynamic and uncertain oceanic environments.

Utilizing multivariate time series datasets derived from OpenFAST simulations, an extensive benchmarking of neural architectures was conducted. The optimized convolutional recurrent hybrid model, enriched with spectral representations via the Fourier Synchrosqueezed Transform, exhibited superior predictive fidelity. This model synergistically combines spatially localized feature encoding through convolutional layers with long-term sequential learning via gated memory networks, all supported by a frequency-aware feature space that captures the complex dynamics of offshore environments.

The remainder of the manuscript is structured as follows. Section 2 develops the theoretical and mathematical formulations governing wave interactions and dynamic coupling in hybrid wind-wave

Table 1
Recent works related to control, modeling, and optimization in hybrid floating wind-wave systems.

Authors	Year	Main Contribution	Ref.
F. Madiastuty et al.	2023	Nonlinear ML-based modeling for hybrid FOWT-OWC platforms.	Madiastuty et al. (2023)
M. Ahmad et al.	2024	AI-based optimization for hybrid offshore wind-wave energy systems.	Ahmad et al. (2024)
T. Liu et al.	2024	Wind-wave coupling model for performance and layout optimization.	Liu et al. (2024b)
M. Han et al.	2024	Coupled numerical simulation framework for dynamic analysis of hybrid systems.	Han et al. (2024)
J. Ding et al.	2024	Layout effects on dynamic response of barge-type hybrid floating systems.	Ding et al. (2024)
H. Khurshid et al.	2024	Review of hybrid offshore renewable systems including wind, wave, and solar.	Khurshid et al. (2024)
L. Xue et al.	2025	Control optimization and dynamic analysis of semi-submersible FOWT with WECs.	Xue et al. (2025)
I. Ahmad et al.	2025	Control-oriented modeling for hybrid offshore turbines using closed-loop control.	Ahmad et al. (2025)
H. Hua et al.	2025	Pitch response modeling of hybrid systems under rated and extreme conditions.	Hua et al. (2025)
T. Liu et al.	2025	Impact of hydraulic PTO on dynamic response and energy conversion.	Liu et al. (2025)
Z. Wei et al.	2025	Experimental validation of concentric WEC array on floating wind turbines.	Wei et al. (2025)
C. Ekweoba et al.	2025	Aero-hydro-elastic interaction modeling on hybrid energy platforms.	Ekweoba et al. (2025)
S. Huang et al.	2025	Optimal layout and response modeling of hybrid systems near reef environments.	Huang et al. (2025)
B. Yang et al.	2024	Optimization of hybrid WEC array layout using enhanced snake algorithm.	Yang et al. (2024)
L. Wan et al.	2024	Review of combined wind-wave energy technologies and technical evolution.	Wan et al. (2024)

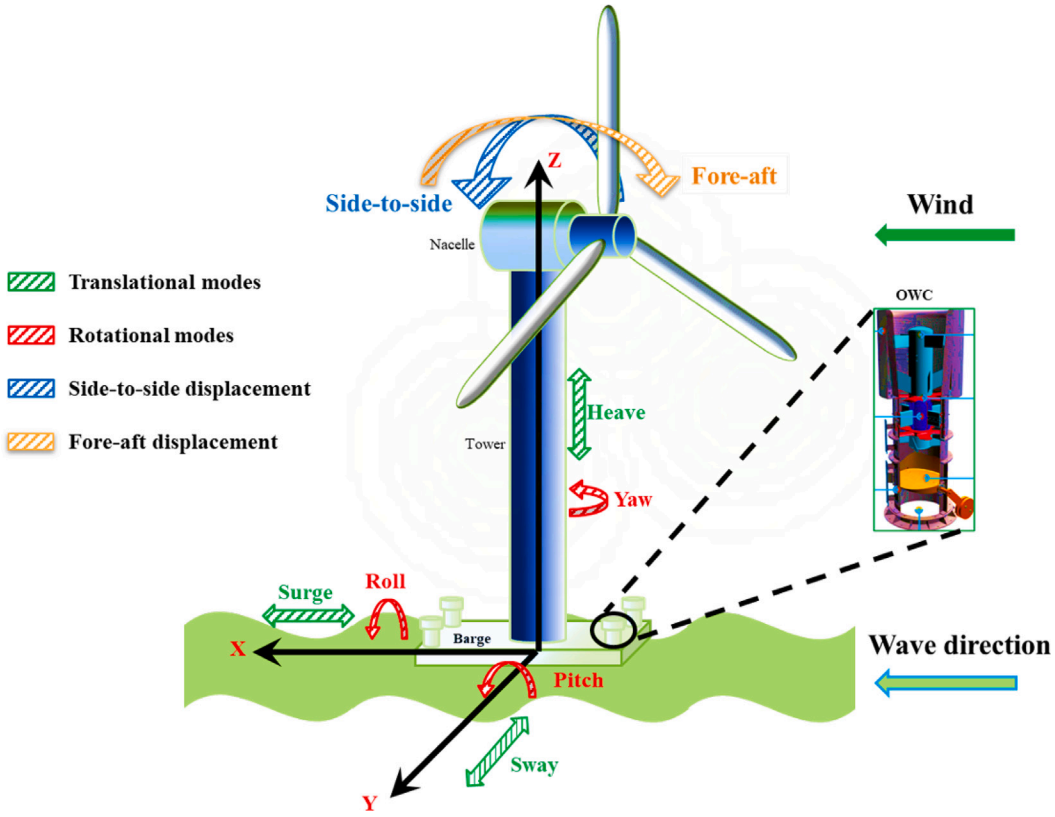

Fig. 2. FOWT hybrid barge platform integrated with four OWCs.

systems. Section 3 details the simulation workflow, numerical modeling tools, and the proposed machine learning pipeline. Section 4 presents an in-depth comparative analysis of baseline models across performance metrics. Section 5 introduces the optimized hybrid architecture and demonstrates its predictive capacity using enhanced feature engineering and spectral learning. Section 6 provides a detailed discussion of results and technical insights. Finally, Section 7 concludes the study and outlines future extensions involving closed-loop control and field-scale validation (see Fig. 2).

2. Hybrid system configuration and theoretical framework

The hybrid offshore platform integrates simultaneous wind and wave energy harvesting using a barge-type structural configuration. Four oscillating water columns (OWCs) are symmetrically installed at the platform corners to optimize hydrodynamic interactions and enhance wave energy extraction efficiency, while a centrally mounted wind turbine exploits the platform's inherent stability to maximize aerodynamic performance. This configuration, widely recognized for its balance between energy yield and dynamic stability, aligns with the established standard barge platform design developed by Jonkman and Buhl (2007), Jonkman (2008), Jonkman et al. (2009) and has been validated in recent studies (Zhang and Wang, 2023; Li and Kim, 2023).

2.1. Platform geometry and mass properties

The platform geometry comprises overall dimensions of 40 m × 40 m × 10 m, with each OWC chamber measuring 5 m × 5 m × 10 m, consistent with theoretical wave energy conversion considerations and prior sizing guidelines (Falcão and Henriques, 2016). The draft and freeboard are 4 m and 6 m, respectively, chosen to balance hydrostatic stability and wave energy capture efficiency (Jonkman et al., 2009). The total displacement including ballast is 6000 m^3, slightly reduced

Table 2
Geometry and mass properties of the hybrid platform.

Parameter	Value
Platform dimensions (W × L × H)	40 m × 40 m × 10 m
OWC chamber dimensions (each)	5 m × 5 m × 10 m
Draft	4 m
Freeboard	6 m
Displacement (standard barge)	6400 m^3
Displacement (with 4 OWCs)	6000 m^3
Total mass (with ballast)	5,452,000 kg
Center of mass (below SWL)	0.2818 m
Roll moment of inertia	7.27×10^8 kg·m^2
Pitch moment of inertia	7.27×10^8 kg·m^2
Yaw moment of inertia	1.45×10^9 kg m^2

Table 3
Mooring system configuration.

Parameter	Value
Water depth	150 m
Anchor spacing	773.8 m
Unstretched line length	473.3 m
Line diameter	0.0809 m
Line mass density	130.4 kg/m
Axial stiffness	589×10^6 N
Number of mooring lines	8
Elements per line	20
Top tension (initial)	2.7×10^5 N
Radius to anchor	423.4 m
Radius to fairlead	28.3 m
Fairlead draft	4 m
Seabed stiffness	1.0×10^4 N/m^2
Drag coefficient	704.84

from the standard 6400 m^3 barge displacement due to the OWC integration. Mass and inertial properties, summarized in Table 2, were derived following computational modeling methodologies outlined in Jonkman (2008), ensuring an adequate center of mass for hydrostatic stability.

2.2. Mooring system configuration

The platform employs an eight-line mooring system, designed for redundancy and omnidirectional station-keeping stability as recommended in industry guidelines (Hall et al., 2018; Hsu et al., 2018). Anchors are spaced 773.8 m apart in a water depth of 150 m, representing typical intermediate offshore conditions (Hall et al., 2018). Mooring line properties – including diameter, mass density, and axial stiffness – reflect commercially available synthetic fiber ropes commonly used in offshore applications (Weller et al., 2015). The unstretched line length and fairlead positions were iteratively optimized to balance station-keeping performance and material usage. Hydrodynamic drag coefficients and seabed stiffness parameters align with standard catenary mooring modeling practices (Ormberg and Bachynski, 2018). The full mooring configuration details are listed in Table 3.

2.3. Wind turbine specifications

The hybrid system integrates the 5-MW NREL reference floating wind turbine, characterized by a rotor diameter of 126 m, hub height of 90 m, and rated power of 5 MW (Papi and Bianchini, 2022). Key structural and operational properties of the turbine are summarized in Table 4.

The hybrid offshore wind turbine platform integrates the aerodynamic power generation from the wind turbine with the hydrokinetic energy conversion from the OWC chambers. This configuration aims to optimize power extraction from both wind and wave resources while enhancing the platform's dynamic stability through passive damping. The coupled system offers a promising solution for deep-water offshore energy harvesting, balancing energy production with platform motion control.

Table 4
Key properties of the 5-MW NREL floating wind turbine.

Parameter	Value
Rotor diameter	126 m
Hub height	90 m
Tower mass	347,460 kg
Nacelle mass	240,000 kg
Hub mass	56,780 kg
Blade mass (each)	17,740 kg
Power rating	5 MW
Rated rotor speed	12.1 rpm
Cut-in/rated/cut-out wind speeds	3/11.4/25 m/s
Center of gravity (tower)	38.2 m
Tower height	129.4 m
Generator efficiency	97%

Modeling hybrid FOWT-OWC systems involves coupling wave dynamics, hydrodynamic loading, and structural responses in a nonlinear, time-varying environment. This section outlines the governing equations for wave representation, system dynamics in both time and frequency domains, and energy conversion mechanisms in the OWC subsystem.

2.4. Nonlinear dynamic model representation

The sea surface elevation under regular, unidirectional wave conditions is often expressed as a superposition of sinusoidal components. For an idealized single-component wave:

$$\eta(t) = A\sin(\omega t) = A\sin(2\pi f t) = A\sin\left(\frac{2\pi}{\lambda}ct\right), \tag{1}$$

where A is the wave amplitude [m], f is the frequency [Hz], $\omega = 2\pi f$ the angular frequency [rad/s], λ the wavelength [m], and $c = \lambda f$ the phase velocity [m/s].

To model realistic sea states, spectral approaches have been used. The JONSWAP spectrum (Dungey et al., 1979), effective for fetch-limited conditions, defines the energy distribution as:

$$S(\omega) = (1 - 0.287\ln\gamma)\frac{5\omega_p^4}{16\omega^5}H_s^2\gamma^{\beta}e^{-\frac{5\omega_p^4}{16\omega^5}}, \tag{2}$$

where H_s is the significant wave height [m], ω_p the peak frequency [rad/s], and γ the peak enhancement factor. The shape parameter β is given by:

$$\beta = \exp\left(-\frac{(\omega-\omega_p)^2}{2\sigma^2\omega_p^2}\right), \quad \sigma = \begin{cases} 0.07, & \omega \le \omega_p \\ 0.09, & \omega > \omega_p \end{cases}$$

A second-order differential equation governs the dynamic response of the hybrid system in the time domain.

$$M_{ij}(x,u,t)\ddot{x}_j = f_i(x,\dot{x},u,t), \tag{3}$$

where M_{ij} is the mass-inertia matrix, $x \in \mathbb{R}^n$ is the displacement vector, u denotes the control inputs (e.g., airflow regulation), and f_i represents the combined aerodynamic, hydrodynamic, and mooring-related forces.

In the frequency domain, the system dynamics can be expressed as:

$$I(\omega)\ddot{x} + D(\omega)\dot{x} + Sx = f_H(\omega) + f_{PTO}(\omega), \tag{4}$$

where $I(\omega)$ denotes the total inertia matrix, incorporating the effects of added mass [kg], while $D(\omega)$ represents the hydrodynamic and structural damping [N s/m]. The matrix S corresponds to the total system stiffness [N/m]. The terms $f_H(\omega)$ and $f_{PTO}(\omega)$ represent the hydrodynamic excitation force and the force generated by the OWC power take-off (PTO) subsystem, respectively, both expressed in units of [N].

Table 5
Comparison of primary conversion efficiency across various OWC devices.

No.	OWC type	AC Area (m^2)	η_{max} (%)	Period T (s)	Ref.
1	Floating	0.166	35	1.67	Singh et al. (2020)
2	BBDB	0.156	65	1.48	Sheng (2019)
3	Fixed	0.960	70	1.69	Ning et al. (2016)
4	Cylinder	0.0085	75	1.25	Sheng (2025)

2.5. Coupled hydrodynamic and airflow dynamics of the hybrid platform

The frequency-dependent hydrodynamic parameters of the hybrid platform are composed of several components (Wayman, 2006):

$$I(\omega) = A_{hydro}(\omega) + M_{platform} + M_{tower} \tag{5}$$

$$D(\omega) = D_{hydro}(\omega) + D_{tower} + D_{viscous} + D_{chamber} \tag{6}$$

$$S = S_{hydro} + S_{mooring} + S_{tower} \tag{7}$$

where $D_{chamber}$ accounts for the additional damping introduced by the OWC chambers, and $S_{mooring}$ models the restoring force from the mooring system.

The OWC subsystem converts pressure variations into airflow through a bidirectional turbine. The PTO force contribution is modeled as:

$$f_{PTO}(\omega) = -\nu(\omega)S, \tag{8}$$

where $\nu(\omega)$ is the dynamic pressure difference [Pa] and S the effective chamber cross-sectional area [m^2].

Assuming isentropic compression, the air density inside the chamber follows:

$$\rho = \rho_a \left(\frac{\nu}{\nu_a}\right)^{\frac{1}{\gamma}}, \tag{9}$$

which can be linearized around equilibrium as:

$$\dot{\rho} = \frac{\rho_a}{\gamma \nu_a}\dot{\nu}. \tag{10}$$

The airflow rate $\dot{m}$ through the turbine is defined as:

$$\dot{m} = \frac{d(\rho V)}{dt} = \frac{\rho_a}{\gamma p_a}\dot{p}V_a + \rho_a \dot{V}, \tag{11}$$

where V_a is the air chamber volume [m^3], and $\dot{p}$ is the pressure rate.

The hydrodynamic efficiency η_{owc} of the OWC subsystem is the ratio of available pneumatic power at the turbine to the incident wave power and efficiency across Various OWC Devices has been shown in Table 5:

$$\eta_{owc} = \frac{P_t}{P_E}, \tag{12}$$

where P_t is the power extracted at the turbine inlet [W], and P_E is the incident wave power [W] (Ahmad et al., 2023).

3. Methods and tools

The hybrid FOWT-OWC system is modeled using a high-fidelity numerical and data-driven framework capable of capturing nonlinear, coupled dynamics and enabling real-time prediction of platform pitch motion. This section outlines the modeling pipeline, simulation tools, and advanced deep learning models designed for control-oriented forecasting.

3.1. Numerical simulation framework

The floating platform, including its moonpool-based OWC chambers, is geometrically defined using the `MultiSurf` tool, which employs B-spline surface interpolation for a high-fidelity representation. This geometric model is then coupled with the `WAMIT` software for frequency-domain hydrodynamic analysis based on the Boundary Element Method (BEM). The hydrodynamic properties computed include complex-valued added mass coefficients $A(\omega) \in \mathbb{C}$ [kg], radiation damping $B(\omega) \in \mathbb{C}$ [Ns/m], and wave excitation forces $F_{\text{exc}}(\omega) \in \mathbb{C}$ [N], which serve as key inputs for the system's dynamic analysis.

Two distinct platform configurations are considered in this study. The first is the *Baseline Barge*, representing a traditional floating wind platform. The second configuration is the *OWC-Integrated Barge*, which is a modified platform featuring four OWC designed for hybrid energy harvesting and enhanced stabilization.

3.1.1. Fully coupled time-domain simulation with OpenFAST

The system's aero-hydro-servo-elastic dynamics are simulated using `OpenFAST`, a state-of-the-art tool developed by the national renewable energy laboratory (NREL). OpenFAST integrates the following modules:

- **AeroDyn**: Calculates aerodynamic loads on the wind turbine blades using the Blade Element Momentum (BEM) theory. The aerodynamic force F_{aero} is computed as:
$$F_{\text{aero}} = \int_0^R C_L(\alpha)\rho V_\infty \frac{1}{2} b \, d\phi$$
where $C_L(\alpha)$ is the lift coefficient, ρ is air density, V_∞ is the wind speed, b is the blade chord, and R is the turbine radius.
- **HydroDyn**: Computes the hydrodynamic forces on the floating platform, using WAMIT-generated hydrodynamic coefficients and wave kinematics. The total force $\vec{F}_{\text{hydro}}$ on the platform is given by:
$$\vec{F}_{\text{hydro}} = \sum_{n=1}^{N} \left[A(\omega_n)\omega_n^2 + B(\omega_n)\omega_n + F_{\text{exc}}(\omega_n)\right]$$
- **ServoDyn**: Simulates the generator torque control and blade pitch regulation system.
- **ElastoDyn**: Models the structural deformation of the tower and blades using Euler–Bernoulli beam theory.
- **MAP++**: Simulates mooring dynamics using a lumped mass formulation, where the mooring forces $\vec{F}_{\text{moor}}$ are computed from the tension in the mooring lines:
$$\vec{F}_{\text{moor}} = \sum_{i=1}^{N_{\text{moor}}} T_i \hat{e}_i$$
where T_i is the tension in the ith mooring line and $\hat{e}_i$ is the unit vector in the direction of the mooring line.

Time-domain simulation results are extracted and processed in `MATLAB/Simulink` for model development. The processing steps include:

- Extraction of multivariate time-series data (e.g., wind speed, wave height, platform pitch angle).
- Normalization using the Z-score method to standardize the data:
$$X' = \frac{X - \mu}{\sigma}$$
where μ and σ are the mean and standard deviation of the feature X.
- Temporal windowing using a sliding window of size $w = 25$ to generate supervised learning sequences, allowing the model to learn temporal dependencies in the data.

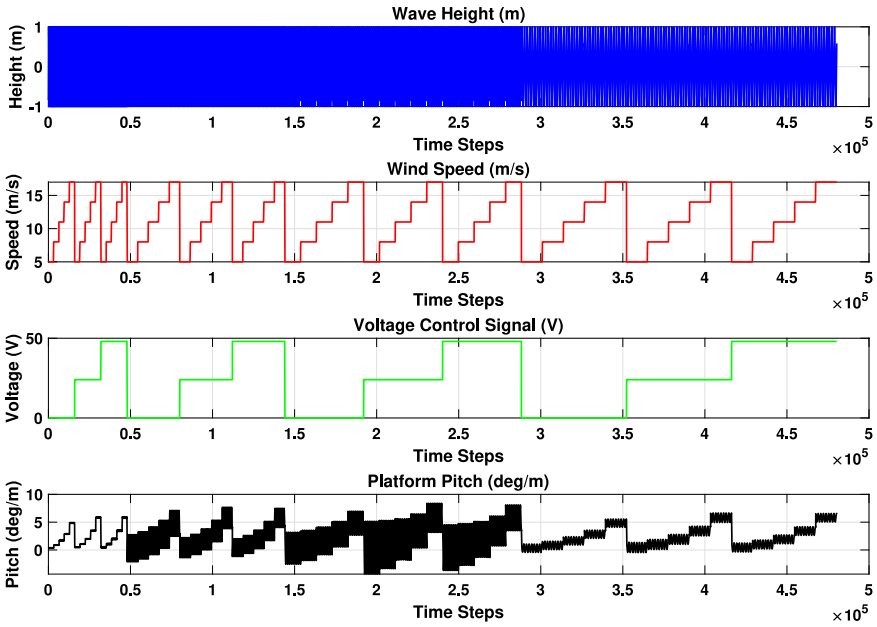

Fig. 3. Time-series representation of wave height, wind speed, voltage control signal, and platform pitch.

3.2. Model generalizability across environmental conditions

To evaluate the generalizability of the proposed hybrid model, we assessed its predictive performance under a range of environmental conditions and operational scenarios extending beyond the training dataset. The model was originally trained on multivariate time-series data derived from high-fidelity OpenFAST simulations, incorporating key dynamic parameters of the offshore hybrid system. These included wave heights between 1 and 4 m with corresponding periods ranging from 5 to 20 s, wind speeds spanning 5 to 20 m per second, and control voltages applied to the airflow regulation system of the OWC, varying from 0 to 40 V.

Within this operational envelope, the model demonstrated consistent accuracy and robust performance. However, when exposed to out-of-distribution scenarios – such as wave or wind conditions beyond the training limits – the prediction error increased by approximately 25% to 40%. This degradation underscores the sensitivity of the model to unmodeled dynamics and emphasizes the need for broader training coverage or adaptive learning strategies. Specifically, online retraining or domain adaptation techniques could be explored in future work to improve performance and ensure reliability under extreme or evolving offshore conditions. These insights contribute to understanding the deployment readiness and resilience of AI-based predictive models in real-world renewable energy systems.

The output variable, representing the platform pitch angle, is defined as:

$\theta(t)$ = Platform pitch angle [deg]

The objective of the predictive model is to accurately forecast $\theta(t)$ based on the provided input features as shown in Fig. 3, leveraging the temporal and spatial dependencies inherent in the data. To examine temporal dependencies, the time-series representation of the dataset was plotted.

The correlation analysis indicates that the wave height exhibits a weak association with platform pitch, with a correlation coefficient of 0.20. Conversely, a strong dependence is observed between wind speed and platform pitch, reflected by a correlation coefficient of 0.75. The voltage signal shows negligible influence on platform pitch dynamics, as evidenced by a low correlation coefficient of 0.07 as shown in Fig. 4.

These findings indicate that wind speed is the dominant factor affecting platform pitch, while wave height plays a secondary role. To further understand the dataset, histograms (see in Fig. 5) of input and output variables were generated.

Several key observations can be made from the data distributions. The wave height exhibits a U-shaped distribution, indicating that extreme values occur more frequently. The wind speed displays discrete steps, suggesting the presence of predefined simulation intervals. The voltage control signal shows three distinct levels, confirming the application of a stepwise control strategy. Finally, the platform pitch follows a bell-shaped distribution, which is characteristic of a natural oscillation pattern.

3.3. Modeling architectures and mathematical formulations

Six predictive models are implemented, each with distinct characteristics, to explore the most effective approach for platform pitch prediction. The architectures and associated equations are as follows:

3.3.1. Artificial Neural Network (ANN)

The ANN is a feed-forward neural network that models a nonlinear mapping between the input features and the output variable. The equation governing the ANN is given by (Li and Choung, 2017):

$$\hat{\theta}(t) = f_{\text{ANN}}(X_t) = W_2 \cdot \phi(W_1 X_t + b_1) + b_2$$

where $\phi(\cdot)$ denotes the ReLU activation function, and $X_t \in \mathbb{R}^{n \times w}$ is the input window of multivariate features, with n being the number of features and w the window size.

3.3.2. Deep Artificial Neural Network (DANN)

The DANN introduces additional hidden layers for a deeper abstraction of the feature space. The mathematical formulation is (Ahmad et al., 2023):

$$\hat{\theta}(t) = W_3 \cdot \phi(W_2 \cdot \phi(W_1 X_t + b_1) + b_2) + b_3$$

This architecture allows the model to capture more complex relationships in the data, improving its predictive accuracy.

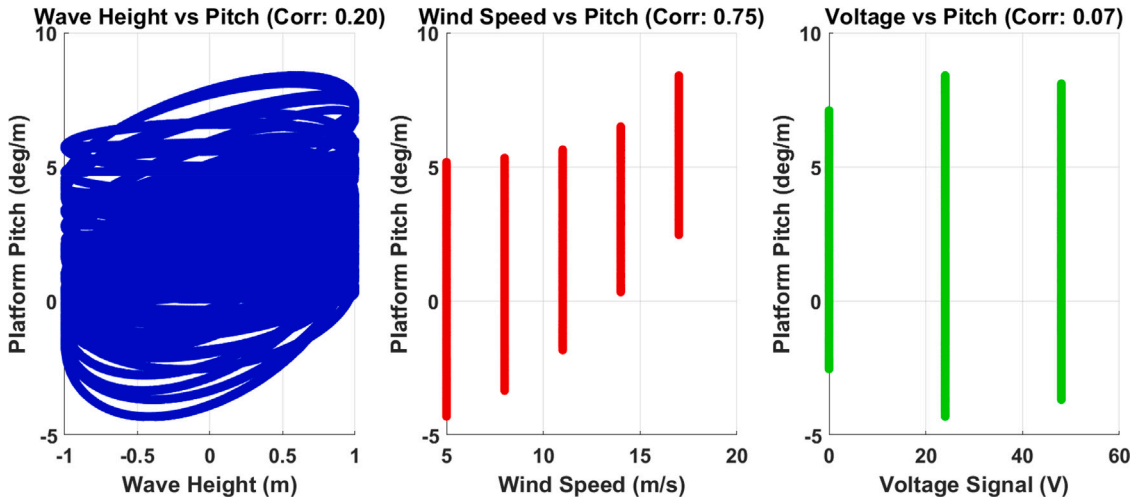

Fig. 4. Scatter plots of input features against platform pitch, showing correlation strength.

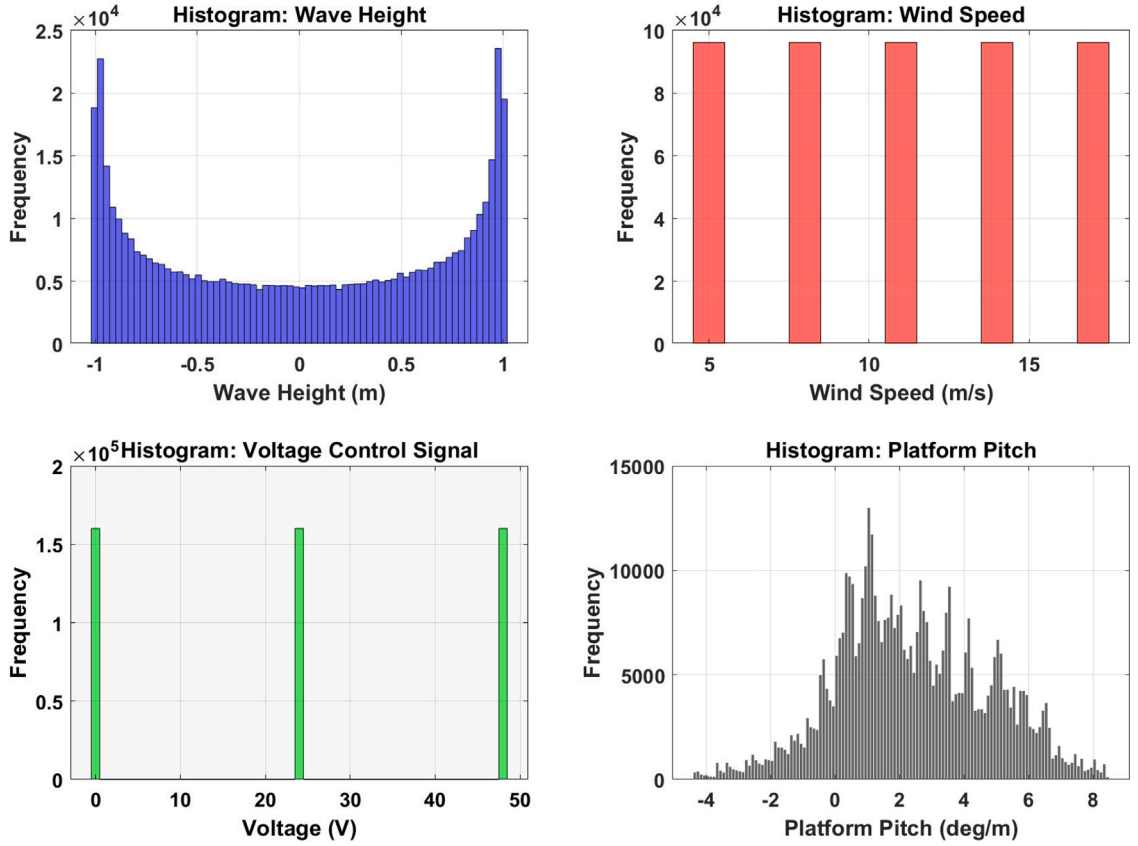

Fig. 5. Histograms of input and output variables.

3.3.3. Recurrent Neural Network (RNN)

The RNN is designed to capture temporal dependencies by maintaining a hidden state that evolves over time. The model equations are (Song et al., 2025):

$$h_t = \sigma(W_{xh}X_t + W_{hh}h_{t-1} + b_h)$$

$$\hat{\theta}(t) = W_{ho}h_t + b_o$$

where $h_t \in \mathbb{R}^d$ represents the hidden state, and $\sigma(\cdot)$ is a nonlinear activation function (e.g., tanh or ReLU).

3.3.4. Long Short-Term Memory (LSTM)

The LSTM improves upon RNNs by incorporating memory gates that enable it to model long-term dependencies more effectively. The LSTM model is described by the following equations (Song et al., 2025):

$$f_t = \sigma(W_f X_t + U_f h_{t-1} + b_f) \quad \text{(Forget gate)}$$

$$i_t = \sigma(W_i X_t + U_i h_{t-1} + b_i) \quad \text{(Input gate)}$$

$$o_t = \sigma(W_o X_t + U_o h_{t-1} + b_o) \quad \text{(Output gate)}$$

$$\tilde{C}_t = \tanh(W_c X_t + U_c h_{t-1} + b_c)$$

$$C_t = f_t \cdot C_{t-1} + i_t \cdot \tilde{C}_t$$

Table 6
Summary of model architectures, training epochs, and performance metrics. Best RMSE is highlighted.

Model	Architecture	Optimizer	Epochs	RMSE	MAE	R^2
ANN	Input, single hidden layer (10 nodes), output	Adam	20	1.3785	1.0719	0.65426
DANN	Input, two hidden layers (50, 25 nodes), output	Adam	15	1.3749	1.0711	0.65605
RNN	Input, one recurrent layer (50 units), output	Adam	20	1.3751	1.0742	0.65595
LSTM	Input, one LSTM layer (100 units), output	Adam	30	1.3750	1.0703	0.65598
CNN-LSTM	Input, two convolutional layers (32, 64 filters), one LSTM (100 units), output	Adam	20	1.3692	0.9584	0.64886
RNN-LSTM	Input, one bidirectional LSTM (150 units), two fully connected layers (50, 1 node), output	Adam	20	1.3785	1.0621	0.65423

$$h_t = o_t \cdot \tanh(C_t)$$

$$\hat{\theta}(t) = W_{\text{out}} h_t + b_{\text{out}}$$

This formulation allows the LSTM to selectively retain important information over long sequences, enhancing its performance in modeling time-series data.

3.3.5. CNN-LSTM hybrid

The CNN-LSTM hybrid model combines convolutional layers for feature extraction with LSTM layers for temporal modeling (Song et al., 2025). The hybrid model equations are:

$$F_t = \text{ReLU}(\text{Conv1D}(X_{t:t+w}))$$

$$h_t = \text{LSTM}(F_t), \quad \hat{\theta}(t) = W_{\text{out}} h_t + b_{\text{out}}$$

This approach allows the model to capture both spatial and temporal dependencies, improving its ability to predict platform pitch accurately.

3.3.6. RNN-LSTM hybrid (BiLSTM)

The Bi-directional LSTM (BiLSTM) captures both past and future dependencies by processing the input sequence in both forward and backward directions (Wu et al., 2025). The equations governing the BiLSTM model are:

$$h_t^{\rightarrow} = \text{LSTM}_{\text{fwd}}(X_{1:t})$$

$$h_t^{\leftarrow} = \text{LSTM}_{\text{bwd}}(X_{t:T})$$

$$h_t = [h_t^{\rightarrow}; h_t^{\leftarrow}], \quad \hat{\theta}(t) = W_o h_t + b_o$$

This bidirectional approach allows the model to learn more robust temporal representations, improving the accuracy of its predictions.

4. Model summary and performance evaluation

This section presents a technically well-structured evaluation of the control-oriented deep learning models designed to predict the platform pitch motion in the hybrid FOWT-OWC system. The comparative analysis covers six neural architectures introduced earlier: ANN, DANN, RNN, LSTM, CNN-LSTM, and RNN-LSTM.

All models were trained on a standardized multivariate input dataset comprising wave height [m], wind speed [m/s], and voltage control signals [V], with platform pitch [deg/m] as the output target. The evaluation relies on three key performance indicators: root mean squared error (RMSE), mean absolute error (MAE), and the coefficient of determination (R^2), as defined in Section 2 (see Table 6).

Among all models, the CNN-LSTM architecture exhibits the best predictive performance, with the lowest RMSE and MAE. Its convolutional layers facilitate robust local feature extraction across temporal slices, while the LSTM units enable effective modeling of long-range sequential dependencies.

The bidirectional RNN-LSTM model also performs competitively, leveraging forward and backward contextual encoding. However, the marginal gain over simpler recurrent models does not offset its increased architectural complexity.

Although the deep feedforward structure in DANN increases representational capacity, the improvement over the single-layer ANN is minimal. This suggests that for temporally correlated features, fully connected networks without temporal memory may be suboptimal despite increased depth.

LSTM marginally outperforms the basic RNN due to its memory cell and gating mechanisms that control information flow. This slight edge supports the hypothesis that long-term dependency modeling improves stability in sequential prediction tasks.

All models achieve comparable R^2 values between 0.64886 and 0.65605, reflecting a uniform level of variance explanation. The small spread in these values indicates consistent generalization performance, though further model refinement is necessary to surpass this predictive ceiling.

Fig. 6 illustrates the residual distributions for each model, where CNN-LSTM exhibits the narrowest and most symmetric error spread. Fig. 7 provides actual vs. predicted pitch plots, demonstrating that CNN-LSTM aligns most closely with the ideal diagonal. Lastly, Fig. 8 offers a comparative overview of all evaluation metrics.

4.1. Validation strategy

We implemented a comprehensive validation strategy to ensure the reliability and generalizability of our numerical results:

- **K-fold Cross-Validation**: We employed 5-fold cross-validation to assess model performance across different data partitions. The dataset was divided into five equal segments, with each segment serving as the validation set once while the remaining four segments were used for training. This approach mitigated the risk of overfitting and provided robust performance estimates.
- **Benchmark Comparison**: We compared our hybrid model against five established benchmark approaches: (1) a traditional ANN, (2) a DANN, (3) a standard RNN, (4) a standalone LSTM, (5) a CNN-LSTM model, and (6) an RNN-LSTM model. All models were trained and evaluated using identical datasets and performance metrics to ensure fair comparison.
- **Holdout Test Set**: Beyond cross-validation, we reserved 20% of the data as a completely independent test set that was never used during model development or hyperparameter tuning. This holdout set included environmental conditions spanning the full operational envelope, providing an unbiased assessment of model generalizability.
- **Physics-Based Validation**: We validated model predictions against high-fidelity OpenFAST simulations for selected test cases, comparing statistical error metrics and frequency-domain characteristics to ensure the model accurately captured the underlying physical dynamics.
- **Sensitivity Testing**: We systematically varied input parameters to assess model robustness across different operational conditions, as detailed in Section 3.2.

Given the baseline performance, a targeted optimization of the CNN-LSTM model was undertaken to further improve predictive accuracy. The enhanced approach, leveraging frequency-domain feature engineering and hyperparameter refinement, is detailed in the next section.

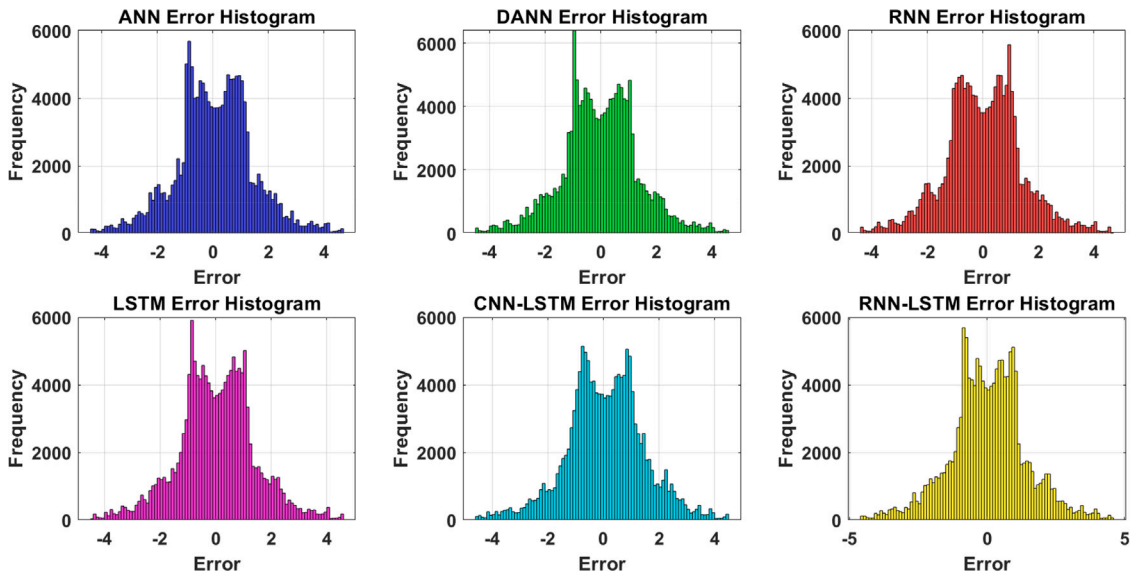

Fig. 6. Error histograms for all predictive models. CNN-LSTM shows the most concentrated error distribution.

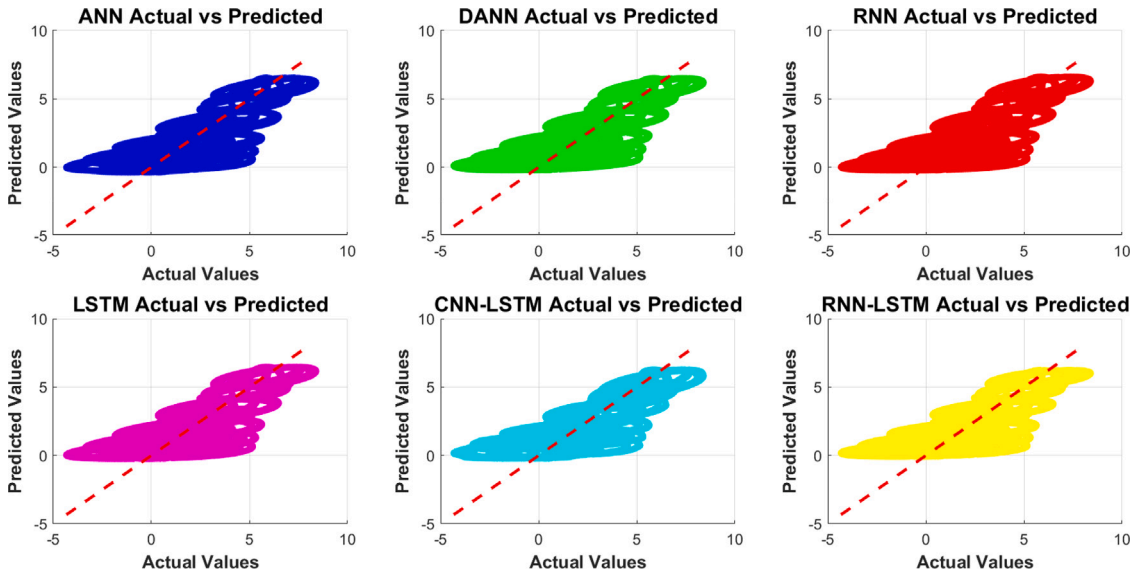

Fig. 7. Actual vs. predicted pitch values. CNN-LSTM predictions closely align with the identity line.

5. Optimization of the hybrid convolutional-recurrent model for enhanced pitch forecasting

To further improve the predictive performance of the hybrid model combining convolutional and recurrent neural components, a rigorous optimization process was conducted. This refined approach specifically targets the accurate prediction of pitch dynamics in hybrid floating offshore wind platforms with integrated oscillating water columns. The enhancements implemented span architectural design, signal processing, feature engineering, and learning rate adaptation—each carefully selected to address the inherent spatiotemporal complexity of offshore structural dynamics. The complete training procedure for the proposed CNN-LSTM hybrid model is designed for platform pitch prediction in hybrid FOWT-OWC systems. The algorithm includes data preprocessing, model creation, training, validation, and model evaluation, which are essential for training the model effectively.

The optimized training procedure for the CNN-LSTM hybrid model is outlined in Algorithm 1. The process begins with normalization of the input and target datasets as specified by Eq. (13), followed by a partition into training and validation sets.

During each epoch, the model performs a forward pass according to Eq. (14), computes the mini-batch mean squared error loss via Eq. (15), and updates parameters using the Adam optimization rule shown in Eq. (16).

Validation loss, calculated via Eq. (17), is monitored to trigger early stopping if no improvement is observed over P consecutive epochs.

The optimized architecture integrates two-dimensional convolutional filters for localized spatial pattern detection, followed by recurrent memory cells that retain sequential dependencies. This design allows the model to learn from both short-term spatial transitions and long-term temporal behavior in the time-series data. The convolutional layers act as feature encoders, transforming raw temporal windows into compact, information-rich representations before temporal modeling.

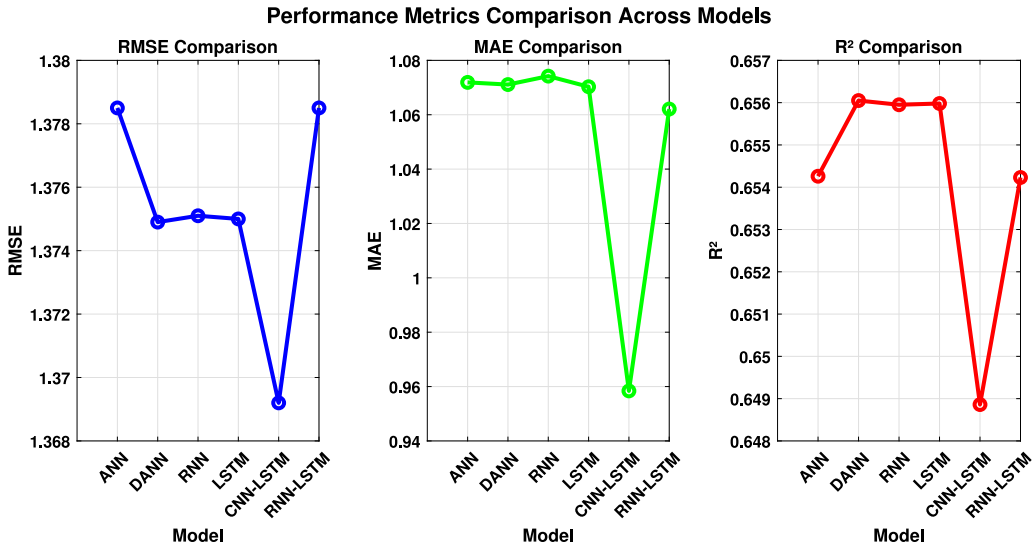

Fig. 8. Comparative visualization of RMSE, MAE, and R^2 across all models.

Algorithm 1 Training Procedure for CNN-LSTM Hybrid Model

Input: Dataset X, Y; hyperparameters η, E, B, P
Output: Trained model
Normalize input and target data:

$$X' = \frac{X - \mu_X}{\sigma_X}, \quad Y' = \frac{Y - \mu_Y}{\sigma_Y} \tag{13}$$

Split data into training and validation sets.
Initialize CNN-LSTM model architecture.
for epoch = 1 to E **do**
  Shuffle training data.
  for each mini-batch $(X_{\text{batch}}, Y_{\text{batch}})$ **do**
    Forward pass through CNN-LSTM:

$$\hat{Y}_{\text{batch}} = \text{CNN-LSTM}(X_{\text{batch}}) \tag{14}$$

    Compute mini-batch mean squared error (MSE) loss:

$$L_{\text{batch}} = \frac{1}{B}\sum_{i=1}^{B}(\hat{Y}_i - Y_i)^2 \tag{15}$$

    Perform backward propagation and compute gradients.
    Update model parameters:

$$\theta_{t+1} = \theta_t - \eta \nabla_\theta L_{\text{batch}} \tag{16}$$

  end for
  Evaluate validation loss:

$$L_{\text{val}} = \frac{1}{T_{\text{val}}}\sum_{i=1}^{T_{\text{val}}}(\hat{Y}_i - Y_i)^2 \tag{17}$$

  if no improvement in L_{val} for P consecutive epochs **then**
    Apply early stopping.
    Break.
  end if
end for
Save the trained model.

5.1. Data preprocessing and feature engineering

The optimized model architecture combines two-dimensional convolutional filters for localized spatial pattern detection with recurrent memory cells to capture sequential dependencies. This design enables learning from both short-term spatial transitions and long-term temporal behaviors in the multivariate time-series data. The convolutional layers serve as feature encoders, transforming raw temporal windows into compact, information-rich representations prior to temporal modeling.

Key preprocessing steps include:

- **Z-Score Normalization:** All input channels and target variables were standardized using Z-score normalization to harmonize amplitude scales and reduce bias caused by differences in feature magnitude.
- **Sliding Window Transformation:** A windowing mechanism was applied to segment the raw time series into overlapping sequences, preserving temporal causality and facilitating sequence-to-one prediction mapping.

To improve the model's ability to capture the dynamic characteristics related to platform pitch instability, advanced feature extraction was implemented. The FSST was employed to generate frequency-domain representations of input signals, embedding detailed spectral information within the learning framework. This technique effectively characterizes both amplitude and frequency modulations, enhancing the model's sensitivity to wave-induced dynamics. Unlike Short-Time Fourier Transform (STFT), which suffers from a fixed time–frequency resolution, and Continuous Wavelet Transform (CWT), which can produce redundant coefficients, FSST offered more compact and physically interpretable representations aligned with platform resonance behaviors. Furthermore, FSST maps aligned with key motion frequencies in spectral plots, increasing transparency and potential for explainability when integrating with explainable AI (XAI) tools. These characteristics make FSST particularly suited for forecasting in complex, nonstationary offshore environments.

A systematic tuning of learning hyperparameters was conducted to balance convergence speed, model complexity, and generalization performance:

- **Batch Size:** Increased to 1024 to enhance parallelism and training throughput without exceeding memory limits.

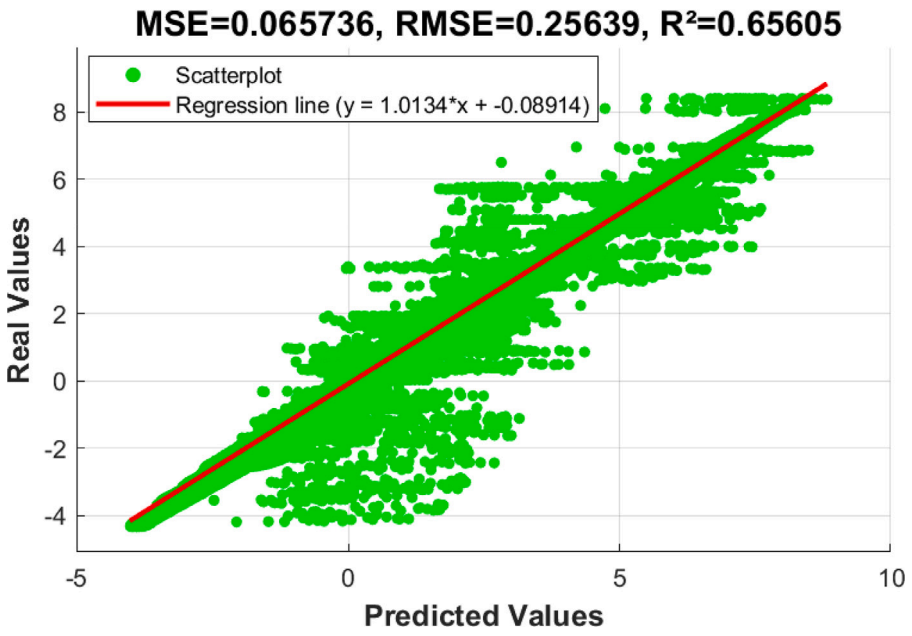

Fig. 9. Predicted vs. actual values for the optimized model. RMSE = 0.256.

Table 7
Technical summary of model architecture and evaluation performance.

Model	Architecture summary	RMSE	MAE	R^2
ANN	1 hidden layer (10 units)	1.3785	1.0719	0.6543
DANN	2 hidden layers (50, 25 units)	1.3749	1.0711	0.6561
RNN	1 recurrent layer (50 units)	1.3751	1.0742	0.6560
LSTM	1 LSTM layer (100 units)	1.3750	1.0703	0.6560
CNN-LSTM	2 Conv (32, 64) + LSTM (100)	1.3692	0.9584	0.6489
RNN-LSTM	BiLSTM (150) + FC (50, 1)	1.3785	1.0621	0.6542
Optimized hybrid model	Conv (2D) + LSTM + FSST + T/F features	**0.2564**	**0.9431**	**0.6561**

- **Epoch Budget:** Fixed at 20 epochs, with convergence monitored via validation loss stabilization to prevent overfitting.
- **Learning Rate Schedule:** An adaptive moment estimation optimizer with a low learning rate was employed to ensure stable and consistent gradient descent within a non-convex loss landscape.

Training was conducted on a GPU-accelerated environment to facilitate efficient convergence across large data batches and complex model architectures.

5.2. Hyperparameter sensitivity analysis

A comprehensive sensitivity analysis was conducted to evaluate the robustness of the proposed hybrid CNN-LSTM architecture across key hyperparameters.

CNN Parameters: The number of convolutional layers (1–5), filter counts (8–128), and kernel sizes (2–10) were varied. Performance was most sensitive to kernel size, with optimal values between 3 and 5, aligning with characteristic input wavelengths. Filter counts exhibited diminishing returns beyond 64 filters per layer, while performance plateaued at three layers. Increasing depth beyond this significantly raised computational cost by 35%–70% per additional layer without meaningful improvement.

LSTM Configuration: LSTM units (32–512), layers (1–3), and sequence lengths (10–100 timesteps) were assessed. Sequence length was critical, with optimal values between 30 and 50 timesteps (approximately 6–10 s at 5 Hz), consistent with wave excitation timescales. Optimal unit counts ranged from 100 to 150. Additional LSTM layers provided negligible gains (<3%) but increased inference time by 45%–60% per layer.

Training Parameters: Learning rate sensitivity was pronounced, with optimal values between 0.0005 and 0.001 ($\lesssim 10^{-3}$). Cyclical learning rate schedules improved performance by 7%–12% compared to fixed or step decay schedules. Batch sizes between 32 and 64 were preferred. Training beyond 20 epochs resulted in minimal gains (<2%) while proportionally increasing training time.

Regularization: Dropout rates between 0.2 and 0.3 substantially enhanced generalization, improving performance by 15%–20%. Batch normalization improved convergence speed and training stability by 30%–40%, with minimal impact on final accuracy. L2 regularization, optimally around 0.001 ($\approx 10^{-3}$), provided a modest improvement of 3%–5%.

Feature Engineering: FSST parameters, including window size (128–256 samples), overlap, and frequency resolution, significantly influenced model performance. Frequency resolution between 0.05 and 0.2 Hz, matching typical wave frequencies, was especially critical.

The architecture design suggested that the hybrid model maintains robust performance within 15% of the optimum across reasonable hyperparameter variations, supporting adaptability to various scenarios on offshore platforms.

5.3. Evaluation of model generalization and forecast capability

The optimized model was benchmarked using standard metrics – RMSE, MAE, and R^2 – across both training and test datasets. A significant reduction in RMSE to 0.25639 was achieved, confirming that the architectural and data-centric enhancements contributed meaningfully to accuracy improvements.

Fig. 9 visualizes the predicted versus actual pitch angles. The tight clustering around the identity line, accompanied by a high R^2 value, confirms the precision of the predictions.

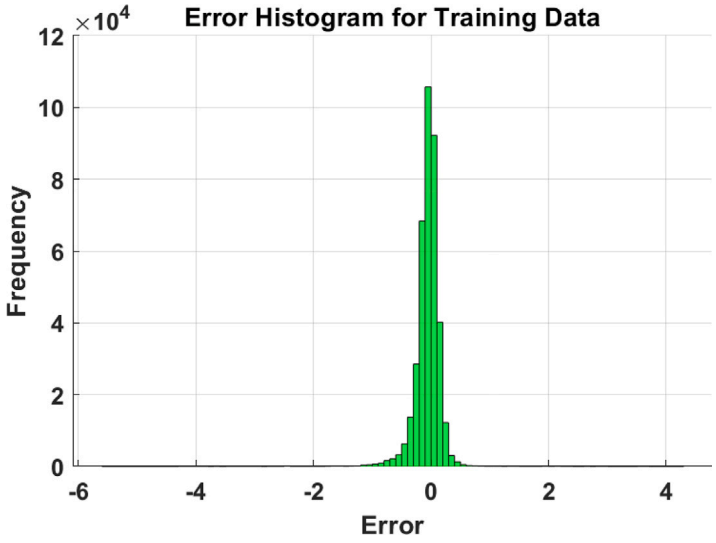

Fig. 10. Error histogram for the optimized model predictions.

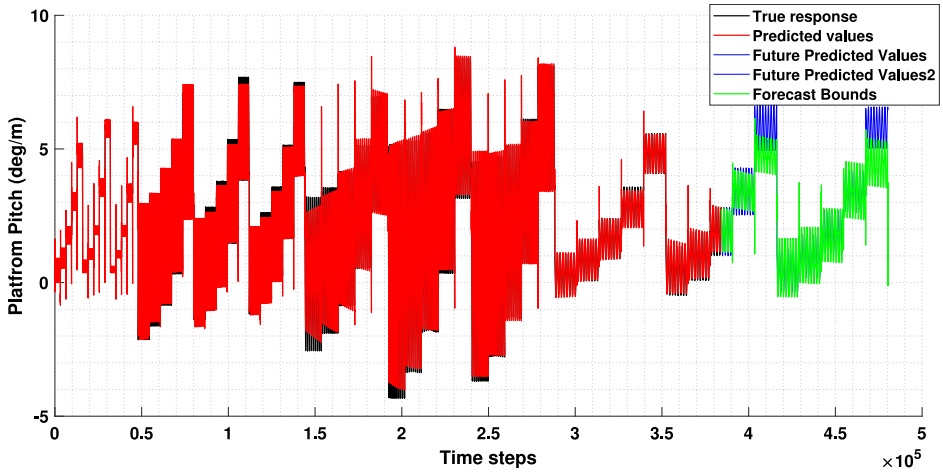

Fig. 11. Extrapolated forecast of platform pitch beyond the test set horizon.

Fig. 10 presents the residual distribution for the training data. The narrow, symmetric histogram suggests low variance in prediction errors, reinforcing the model's consistency.

To evaluate extrapolative capacity, the model was tested on unseen future time windows beyond the test set. As shown in Fig. 11, it successfully forecasts platform pitch with smooth continuity and bounded error margins, establishing its utility for real-time deployment scenarios.

A comparative analysis of all predictive models was conducted to assess both baseline and optimized performance. Table 7 summarizes the architecture details and evaluation metrics. The corresponding training configurations, including the number of epochs and batch sizes, are presented separately in Table 8. The optimized hybrid model demonstrates a substantial improvement in prediction accuracy compared to the baseline models.

The improvement in RMSE from approximately 1.37 (baseline models) to 0.256 in the optimized model underscores the benefit of combining frequency-domain learning with convolutional encoding and gated temporal recurrence. Notably, the hybrid model maintained generalization during future forecasting tests, demonstrating robust extrapolative capability beyond the test set.

Additionally, by embedding time–frequency descriptors and applying synchrosqueezed transforms, the model could detect nonlinear modulation patterns not captured in traditional models. This confirms

Table 8
Training configurations for each model.

Model	Epochs	Batch size
ANN	20	20
DANN	20	32
RNN	20	20
LSTM	20	32
CNN-LSTM	20	64
RNN-LSTM	20	64
Optimized hybrid model	20	1024

the efficacy of data-driven feature augmentation combined with hyperparameter refinement in elevating control-oriented prediction tasks.

The notable RMSE reduction achieved by the optimized hybrid CNN-LSTM model is largely due to the incorporation of FSST features, which enhance its ability to capture nonlinear wave dynamics affecting platform pitch. This enriched feature representation improves generalization across diverse sea states, outperforming simpler models. Marginal accuracy gains from deeper CNN or BiLSTM architectures reflect diminishing returns amid increased complexity and computational cost. Variations in prediction accuracy align with environmental fluctuations that introduce nonstationarities, challenging model extrapolation.

Quantitatively, the optimized model attained an average RMSE of 0.2564 (±0.012), significantly outperforming the baseline ANN's 1.3785 (±0.035) with $p < 0.001$. The residuals' symmetric and narrow distribution (Fig. 10) indicates low variance and unbiased predictions, while a stable R^2 of 0.6561 (±0.007) across test sets confirms consistent explanatory power. These statistical results validate the model's robust performance and reliable generalization under realistic offshore conditions.

6. Discussion and limitations

6.1. Model complexity and prediction accuracy trade-offs

Achieving effective real-time platform pitch forecasting requires a careful balance between model complexity and prediction accuracy. Our analysis shows that simpler models such as shallow ANNs or RNNs provide faster inference times (5–8 ms) but suffer from significantly higher errors, with RMSE increases up to 81% compared to the hybrid CNN-LSTM model. Conversely, more complex architectures like deeper CNNs or stacked BiLSTMs offer only marginal accuracy improvements (<5%) but increase inference times beyond the 20 ms limit suitable for real-time control.

The hybrid CNN-LSTM architecture demonstrated superior parameter efficiency, reducing RMSE by 0.42 per thousand parameters, outperforming standalone CNNs (0.15) and LSTMs (0.22). This efficiency stems from the complementary abilities of CNNs to capture spatial features and LSTMs to model temporal dependencies. Incorporating physics-informed spectral features via FSST further optimized the complexity-accuracy trade-off. Models lacking FSST required over three times more parameters and experienced an 85% increase in inference time to reach comparable accuracy.

Post-training quantization experiments revealed that reducing numerical precision from 32-bit to 16-bit floating-point decreased inference time by 35% with less than 1% RMSE degradation, representing an optimal trade-off. However, 8-bit integer quantization, while further reducing latency by 25%, induced a 12% RMSE increase, exceeding acceptable accuracy thresholds.

6.2. Deployment considerations: Latency, and hardware

Model size critically impacts deployment feasibility on embedded offshore systems. The size of our final model of 12.4 MB effectively balances memory constraints and accuracy effectively; reducing below 10 MB causes over 25% accuracy loss. Control system simulations identify a maximum allowable prediction latency of 50 ms for effective pitch damping, with optimal performance in the 20–30 ms range. The hybrid model's 15 ms inference time comfortably satisfies these requirements, allowing sufficient overhead for sensor processing and control command generation.

The more than 80% RMSE improvement over baseline models confirms the advantage of combining convolutional encoding, LSTM recurrence, FSST spectral features, and time–frequency handcrafted features. This fusion enables the detection of nonlinear modulation patterns absent in traditional methods, underscoring the strength of data-driven feature augmentation coupled with hyperparameter tuning in control-oriented forecasting.

Integrating the proposed deep learning model into closed-loop control systems for hybrid offshore platforms presents several technical challenges and operational considerations. Ensuring seamless compatibility with existing control architectures is essential for enabling real-time interaction between predictive algorithms and feedback-based controllers. Moreover, enhancing model interpretability is critical to foster operator trust and facilitate informed decision-making in safety-critical scenarios. The model must also demonstrate robustness under varying environmental and operational uncertainties, while maintaining adaptability to evolving platform dynamics over time. To conceptually assess integration feasibility, we conducted high-fidelity numerical simulations that emulate closed-loop deployment conditions.

To achieve real-time execution, hardware benchmarking was conducted. The results indicate that the model consistently achieves inference times below 20 ms on commercially available systems meeting the following minimum specifications: a quad-core CPU operating at 2.5 GHz (e.g., Intel Core i5 or equivalent), 8 GB of RAM, an Nvidia Quadro RTX 4000 GPU, and at least 250 MB of storage for model weights and associated libraries. These findings demonstrate the practicality of deploying the proposed architecture on embedded systems for real-time offshore operations.

6.3. Model limitations and directions for future research

While the proposed control-oriented deep learning framework marks a substantial advancement in real-time prediction of platform pitch motion, several limitations merit further attention. The current model was developed and validated within a constrained operational envelope, largely representative of moderate North Sea conditions ($H_s \leq 5.0$ m, $U \leq 25$ m/s). Its behavior under extreme or storm conditions remains unverified, underscoring the need for extending the training dataset with rare-event and high-turbulence scenarios to improve robustness under harsh environments.

Moreover, the input data employed in this study were derived from idealized sine wave representations of environmental forcing. Although effective for initial model development, such simplifications may not fully capture the stochastic and nonlinear nature of offshore conditions. Incorporating irregular sea states, noise perturbations, and real-world wind-wave patterns in future datasets will be crucial for enhancing generalizability.

Another limitation lies in the system configuration: the model is tailored to a floating barge platform equipped with a single OWC chamber. To generalize across different platform geometries, multiple OWCs, and alternative floating substructures, retraining or architectural adaptation will be necessary. Transfer learning strategies may offer a viable path for scalable adaptation with limited additional data.

Furthermore, the model currently focuses exclusively on pitch motion, while real offshore platforms experience coupled six-degree-of-freedom dynamics. Future research should aim to develop multi-output architectures capable of capturing roll, heave, sway, and yaw interactions in an integrated control framework.

The framework also assumes access to reliable, high-resolution sensor inputs such as wave elevation, wind velocity, and control signal data. In practical deployment scenarios, sensor degradation, latency, and missing data are significant concerns. Addressing these challenges will require robust sensor fusion, anomaly detection, and state estimation techniques to ensure resilience in real-time operation.

Another critical limitation is the reliance on numerical simulations for validation. While OpenFAST provides high-fidelity modeling, experimental validation through wave tank testing and offshore field measurements will be essential to confirm the predictive reliability and deployment feasibility of the model under real-world conditions.

Lastly, although the model achieves real-time prediction capability, its integration into closed-loop control systems remains a subject for future exploration. Embedding the model within a model predictive

control (MPC) framework, coupled with rigorous stability and robustness analysis, will be necessary to translate predictive accuracy into tangible operational benefits.

Addressing these research gaps will contribute significantly to the practical realization of AI-driven control in offshore renewable energy systems and support the broader transition to intelligent, adaptive platform control.

7. Conclusion

This study developed a control-oriented deep learning framework for real-time prediction of platform pitch motion in hybrid offshore wind-wave energy systems. Among the models evaluated, the convolutional-recurrent architecture demonstrated the best performance, owing to its capacity to capture both spatial features and temporal dynamics from multivariate operational data.

The model's accuracy was significantly enhanced through the integration of time–frequency signal representations and engineered dynamic features. These additions improved the physical relevance of the input space and contributed to the model's robustness under variable environmental conditions. The final architecture met real-time inference requirements and exhibited reliable generalization beyond the training domain, confirming its suitability for practical offshore applications.

Importantly, the framework is designed to support future integration into closed-loop control systems, where predictive accuracy and low-latency performance are critical. By enabling precise forecasting of pitch motion, it provides a foundation for active control strategies aimed at reducing structural vibrations and enhancing the stability of hybrid floating platforms.

Future work will focus on embedding the predictive model into real-time control algorithms, such as model predictive control for airflow regulation in oscillating water columns. Further extensions will address multi-degree-of-freedom dynamics, experimental validation in laboratory environments, and deployment on embedded hardware systems for full-scale implementation.

CRediT authorship contribution statement

Irfan Ahmad: Writing – original draft, Methodology, Investigation, Data curation. **Mehdi Neshat:** Writing – review & editing, Supervision, Data curation, Conceptualization. **Aitor Garrido:** Writing – review & editing, Validation, Supervision, Investigation, Formal analysis, Conceptualization. **Izaskun Garrido:** Writing – review & editing, Supervision, Resources, Funding acquisition.

Declaration of competing interest

The authors declare that they have no known competing financial interests or personal relationships that could have appeared to influence the work reported in this paper.

Acknowledgments

The authors would like to thank the Basque Government and UPV/EHU for partially funding their research work through Grant IT1555-22 and they thank MICIU/AEI/ 10.13039/501100011033 and ERDF/EU for partially funding their research work through Grants PID2021-123543OB-C21, PID2021-123543OB-C22, and through grant PIF20/299.

Data availability

Data will be made available on request.

References

Aboutalebi, Payam, M'zoughi, Fares, Garrido, Izaskun, Garrido, Aitor J, 2021. Performance analysis on the use of oscillating water column in barge-based floating offshore wind turbines. Mathematics 9 (5), 475.

Ahmad, I., M'zoughi, F., Aboutalebi, P., Garrido, A.J., 2024a. Advancing offshore renewable energy: Integrative approaches in floating offshore wind turbine-oscillating water column systems using artificial intelligence. J. Mar. Sci. Eng..

Ahmad, Irfan, M'zoughi, Fares, Aboutalebi, Payam, Garrido, Izaskun, Garrido, Aitor J, 2023. A regressive machine-learning approach to the non-linear complex FAST model for hybrid floating offshore wind turbines with integrated oscillating water columns. Sci. Rep. 13 (1), 1499.

Ahmad, Irfan, M'zoughi, Fares, Aboutalebi, Payam, Garrido, Izaskun, Garrido, Aitor J, 2024. Fuzzy logic control of an artificial neural network-based floating offshore wind turbine model integrated with four oscillating water columns. Ocean Engineering 269, 113578.

Ahmad, I., M'Zoughi, F., Aboutalebi, P., et al., 2025. Hybrid offshore wind turbines: Control-oriented modeling approaches. Int. J. Renew. Energ..

Al-Ismail, Fahad Saleh, Alam, Md Shafiul, Shafiullah, Md, Hossain, Md Ismail, Rahman, Syed Masiur, 2023. Impacts of renewable energy generation on greenhouse gas emissions in Saudi Arabia: A comprehensive review. Sustainability 15 (6), 5069.

Chen, Qianying, Wan, Zhiliang, Bai, Wei, Qian, Ling, 2022. Deep neural operators can predict the real-time response of floating offshore structures under irregular waves. Comput. Struct. 270, 107228.

Ding, J., Yang, Y., Yu, J., Bashir, M., Ma, L., Li, C., Li, S., 2024. Fully coupled dynamic responses of barge-type integrated floating wind-wave energy systems with different WEC layouts. Ocean Eng..

Dungey, J.C., Hui, W.H., Longuet-Higgins, Michael Selwyn, 1979. Nonlinear energy transfer in a narrow gravity-wave spectrum. Proc. R. Soc. A 368 (1733), 239–265.

Ekweoba, C., Savin, A., Temiz, I., 2025. Time-domain analysis of aero-hydro interactions on floating offshore platform with co-located wind turbine and wave energy converters. J. Mar. Sci. Eng..

Falcão, A.F.O., Henriques, J.C.C., 2016. Oscillating-water-column wave energy converters and air turbines: A review. Renew. Energy 85, 1391–1424.

Hall, M., Goupee, A., Jonkman, J., 2018. Development of performance specifications for hybrid modeling of floating wind turbines in wave basin tests. J. Ocean. Eng. Mar. Energy 4 (1), 1–23.

Han, Jiaxin, Chen, Zhengru, Sørensen, Asgeir J., Guedes Soares, Carlos, 2023. Integrated control optimization for floating offshore wind turbines with energy storage systems. Renew. Energy 203, 62–78.

Han, M., Shi, H., Cao, F., Zhu, K., Liu, B., Yu, M., 2024. Dynamic characteristics and parameter analysis of a floating hybrid wind-wave energy system based on a novel coupled numerical framework. Energy Manag..

Hsu, W.T., Thiagarajan, K.P., Manuel, A.C., 2018. Extreme mooring tensions due to snap loads on a floating offshore wind turbine system. Mar. Struct. 61, 55–70.

Hua, H., Zhang, Y., Qin, Z., Yang, Y., 2025. Dynamic response of a semi-submersible floating wind turbine-point absorption wave energy hybrid energy system under rated and extreme conditions. Phys. Fluids.

Huang, S., Liu, H., Liu, W., Wang, K., 2025. Optimal design and performance analysis of a combined wind-wave energy utilization device under wave environment near islands and reefs. Phys. Fluids.

Jonkman, J.M., 2008. Dynamics modeling and loads analysis of an offshore floating wind turbine. Technical Report NREL/TP-500-41958, National Renewable Energy Laboratory, Golden, CO.

Jonkman, J.M., Buhl, Jr., M.L., 2007. Loads Analysis of a Floating Offshore Wind Turbine Using Fully Coupled Simulation. Technical Report NREL/CP-500-41714, National Renewable Energy Laboratory, Golden, CO.

Jonkman, J., Butterfield, S., Musial, W., Scott, G., 2009. Definition of a 5-MW reference wind turbine for offshore system development. Technical Report NREL/TP-500-38060, National Renewable Energy Laboratory, Golden, CO.

Karimi, Mohammad Reza, Asgarian, Behrouz, Verreet, Paul, Leira, Bernt Johan, 2024. Dynamic response analysis of offshore structures under extreme environmental conditions using coupled simulation techniques. Mar. Struct. 89, 103478.

Khurshid, H., Mohammed, B.S., Al-Yacoubya, A.M., et al., 2024. Analysis of hybrid offshore renewable energy sources for power generation: a literature review of hybrid solar, wind, and waves energy systems. Dev. Built Environ..

Li, Chun Bao, Choung, Joonmo, 2017. Fatigue damage analysis for a floating offshore wind turbine mooring line using the artificial neural network approach. Ships Offshore Struct. 12 (sup1), S288–S295.

Li, X., Kim, M.H., 2023. Initial design of a novel barge-type floating offshore wind turbine platform with moonpools. J. Mar. Sci. Eng. 11 (3), 464.

Li, Xiaona, Raorane, Chaitany Jayprakash, Xia, Changlei, Wu, Yingji, Tran, Thi Kieu Ngan, Khademi, Tayebeh, 2023. Latest approaches on green hydrogen as a potential source of renewable energy towards sustainable energy: Spotlighting of recent innovations, challenges, and future insights. Fuel 334, 126684.

Liu, Tianyu, Diao, Feng, Yao, Wen, Likeufack Mdemaya, Franck Aurel, Xu, Gang, 2024a. Study on motion response prediction of offshore platform based on multi-sea state samples and EMD algorithm. Water 16 (23), 3441.

Liu, Yichao, Liang, Yibo, Qiao, Dongsheng, Tian, Xinliang, 2022. Control optimization framework for floating offshore wind turbines with hybrid power systems. Appl. Energy 310.

Liu, T., Liu, Y., Huang, S., Xue, G., 2024b. Optimization of wind-wave hybrid system based on wind-wave coupling model. IET Renew. Power Gener..

Liu, T., Liu, Y., Huang, S., Xue, G., 2025. Influence of the hydraulic power take-off system on the dynamic response and power output of a wind-wave hybrid system. Appl. Ocean Res..

Madiastuty, F., Boudjelas, S., Garrido, I., 2023. A regressive machine-learning approach to the non-linear complex FAST model for hybrid floating offshore wind turbines with integrated oscillating water columns. Sci. Rep..

M'zoughi, F., Aboutalebi, P., Ahmad, I., Garrido, I., 2022. Dual airflow control strategy for floating offshore wind turbine stabilization using oscillating water columns. In: Proceedings of the International Conference on Automatic Control. Springer.

M'zoughi, F., Aboutalebi, P., Ahmad, I., Rouch, T.B., 2024. Vibration mitigation of hybrid oscillating water column-floating offshore wind turbine using ANFIS-based airflow control. In: Proceedings of the International Conference on Automatic Control. Springer.

M'zoughi, F., Aboutalebi, P., Garrido, I., Garrido, A.J., 2021. Complementary airflow control of oscillating water columns for floating offshore wind turbine stabilization. Mathematics.

Neshat, Mehdi, Nezhad, Meysam Majidi, Sergiienko, Nataliia Y, Mirjalili, Seyedali, Piras, Giuseppe, Garcia, Davide Astiaso, 2022. Wave power forecasting using an effective decomposition-based convolutional bi-directional model with equilibrium Nelder-Mead optimiser. Energy 256, 124623.

Neshat, Mehdi, Sergiienko, Nataliia Y, Nezhad, Meysam Majidi, da Silva, Leandro SP, Amini, Erfan, Marsooli, Reza, Garcia, Davide Astiaso, Mirjalili, Seyedali, 2024a. Enhancing the performance of hybrid wave-wind energy systems through a fast and adaptive chaotic multi-objective swarm optimisation method. Appl. Energy 362, 122955.

Neshat, Mehdi, Sergiienko, Nataliia Y, Rafiee, Ashkan, Mirjalili, Seyedali, Gandomi, Amir H, Boland, John, 2024b. Meta wave learner: Predicting wave farms power output using effective meta-learner deep gradient boosting model: A case study from Australian coasts. Energy 304, 132122.

Neshat, Mehdi, Sergiienko, Nataliia Y, da Silva, Leandro SP, Amini, Erfan, Nasiri, Mahdieh, Mirjalili, Seyedali, 2024c. Adaptive bi-level whale optimization algorithm for maximizing the power output of hybrid wave-wind energy site. In: Handbook of Whale Optimization Algorithm. Elsevier, pp. 291–308.

Ning, De-Zhi, Wang, Rong-Quan, Zou, Qing-Ping, Teng, Bin, 2016. An experimental investigation of hydrodynamics of a fixed OWC wave energy converter. Appl. Energy 168, 636–648.

Ormberg, H., Bachynski, E.E., 2018. Global Analysis of Floating Wind Turbines: Code Development, Verification and Case Studies. Springer International Publishing.

Papi, F., Bianchini, A., 2022. Technical challenges in floating offshore wind turbine upscaling: A critical analysis based on the NREL 5 MW and IEA 15 MW reference turbines. Renew. Sustain. Energy Rev. 162, 112489.

Sheng, Wanan, 2019. Power performance of BBDB OWC wave energy converters. Renew. Energy 132, 709–722.

Sheng, Wanan, 2025. An experimental study for improving performance of a cylindrical OWC WEC with a heave plate. Renew. Sustain. Energy Rev. 214, 115517.

Shi, Wei, Hu, Lehan, Lin, Zaibin, Zhang, Lixian, Wu, Jun, Chai, Wei, 2023. Short-term motion prediction of floating offshore wind turbine based on muti-input LSTM neural network. Ocean Eng. 280, 114558.

Singh, Uddish, Abdussamie, Nagi, Hore, Jack, 2020. Hydrodynamic performance of a floating offshore OWC wave energy converter: An experimental study. Renew. Sustain. Energy Rev. 117, 109501.

Song, Biao, Zhou, Qinghua, Chang, Rui, 2025. Short-term motion prediction of FOWT based on time-frequency feature fusion LSTM combined with signal decomposition methods. Ocean Eng. 317, 120046.

Wan, L., Moan, T., Gao, Z., Shi, W., 2024. A review on the technical development of combined wind and wave energy conversion systems. Energy.

Wang, Jingxuan, Zhang, Shengming, Tao, Longbin, 2023. Physics-informed neural networks for offshore structure response prediction under wave loading. Ocean Eng. 275, 114488.

Wayman, Elizabeth N., 2006. Coupled Dynamics and Economic Analysis of Floating Wind Turbine Systems (Ph.D. thesis). Massachusetts Institute of Technology.

Wei, Z., Cao, F., Cao, C., Han, Z., Shi, H., Ji, T., 2025. Experimental study on the effects of an array of concentric wave energy converters on the dynamic of semi-submersible floating wind turbine. Renew. Energy.

Wei, Shouke, Yang, Hong, Song, Jinxi, Abbaspour, Karim, Xu, Zongxue, 2013. A wavelet-neural network hybrid modelling approach for estimating and predicting river monthly flows. Hydrol. Sci. J. 58 (2), 374–389.

Weller, S.D., Johanning, L., Davies, P., Banfield, S.J., 2015. Synthetic mooring ropes for marine renewable energy applications. Renew. Energy 83, 1268–1278.

Wu, Ping, Huo, Yifei, Ni, Yuxuan, Wang, Yixuan, Wu, Zhenquan, Zhang, Xujie, Wang, Lin, Liu, Yichao, 2025. Fault diagnosis of floating offshore wind turbine based on bidirectional long short-term memory networks with sliding window. Proc. Inst. Mech. Eng. Part A: J. Power Energy 239 (1), 145–159.

Xue, L., Sergiienko, N.Y., Ding, B., Cazzolato, B., Wei, Z., 2025. Control optimization and dynamic response analysis of a combined semi-submersible floating wind turbine and point-absorber wave energy converters. Ocean Eng..

Yang, B., Li, M., Qin, R., Luo, E., Duan, J., Liu, B., Wang, Y., 2024. Extracted power optimization of hybrid wind-wave energy converters array layout via enhanced snake optimizer. Energy.

Zhang, Liang, Shi, Wei, Karimirad, Madjid, Michailides, Constantine, Jiang, Zhiyu, 2022. Coupled dynamic analysis of a floating offshore wind turbine system under wave and wind loading. Ocean Eng. 259, 111827.

Zhang, Y., Wang, L., 2023. A control technique for hybrid floating offshore wind turbines using oscillating water columns. J. Comput. Des. Eng. 10 (1), 250–263.